Experimental simulation of shift operators in a quantum processor

Xiangyu Kong,[1,*] Shijie Wei,[2,*] Jingwei Wen,[1,3] Tao Xin,[4,5,6,†] and Gui-Lu Long[1,7,‡]

[1]*State Key Laboratory of Low-Dimensional Quantum Physics and Department of Physics, Tsinghua University, Beijing 100084, China*

[2]*IBM Research, Beijing 100085, China*

[3]*Collaborative Innovation Center of Quantum Matter, Beijing 100084, China*

[4]*Shenzhen Institute for Quantum Science and Engineering, Southern University of Science and Technology, Shenzhen 518055, China*

[5]*Center for Quantum Computing, Peng Cheng Laboratory, Shenzhen 518055, China*

[6]*Shenzhen Key Laboratory of Quantum Science and Engineering, Southern University of Science and Technology, Shenzhen 518055, China*

[7]*Tsinghua National Laboratory for Information Science and Technology, Beijing 100084, China*

(Received 9 October 2018; published 22 April 2019)

The ability to implement quantum operations plays a fundamental role in manipulating quantum systems. Creation and annihilation operators which transform one quantum state into another by adding or subtracting a particle are crucial in constructing the quantum description of many-body quantum theory and quantum field theory. Here we present a quantum algorithm to perform the creation and annihilation operators by the linear combination of unitary operations associated with a two-qubit ancillary system. Our method can realize shift operators akin to creation and annihilation operators simultaneously in the subspace of the whole system. A prototypical experiment was performed with a four-qubit liquid-state nuclear magnetic resonance processor, demonstrating the algorithm via full-state tomography. With a postselected probability of about 50%, the shift operators are realized with a fidelity above 96%. Moreover, our method can be employed to quantum random walk in an arbitrary initial state. With the prosperous development of quantum computing, our work provides a quantum control technology to implement nonunitary evolution in a near-term quantum computer.

DOI: 10.1103/PhysRevA.99.042328

I. INTRODUCTION

The non-Hermitian bosonic operators $\hat{a}$ and $\hat{a}^\dagger$ introduced in the harmonic oscillator question are a basic and crucial concept in quantum mechanics, laying the foundation for quadratic quantization [1]. They offer us an alternative way to calculate the harmonic oscillator system without solving the irksome differential equations [2,3]. These bosonic operators also play an important role in many fields of physics such as quantum optics [4], quantum mechanics [1,5], quantum measurement [6], and even quantum chemistry [7]. According to existing research, the annihilation and creation operation could be the foundation to construct an arbitrary quantum state in theory [8]. Considering the hot field of quantum computation and quantum information, it is natural for us to try to realize these operators in a steerable quantum system which can provide us a novel way to design a quantum algorithm. The designed quantum system has difficulty executing a nonunitary operator, which means there will be an obstacle to evolve from the maximum and minimum quantum states to the zero state in the process of realizing creation and annihilation operators. Given the importance of these operators, efficiently performing them with high success probability and fidelity in the quantum process is critical. Recently, much progress was made in both theory and experiment, one aspect of which focuses on realizing the bosonic operations at the single-boson level in an optical system [4]. But it is usually difficult to achieve both high success probability and performance fidelity at the same time. Some improvements have also been made in the trapped-ion system realizing the deterministic addition and near-deterministic subtraction of a bosonic particle with fidelity over 0.9 [9]. However, improvements still need to be made to satisfy higher precision and less required experiment time.

In this paper, we experimentally realize shift operators akin to creation and annihilation operators using the linear combination of unitary operators in a four-qubit liquid-state nuclear magnetic resonance system. The results offer us an increase in both experiment precision and success ratio. The paper is organized as follows: In Sec. II, we introduce the universal theory of how to realize these two nonunitary operators. In Sec. III, we introduce our experimental setups and procedure for choosing a four-qubit sample. Then, we present the experimental results and discuss the consequences. In Sec. IV, we report an application of our algorithm. Last, we close with a conclusion section summarizing the entire work and giving some prospects.

II. THEORY

Quantum mechanically, the creation operator $\hat{a}^\dagger$ and annihilation operator $\hat{a}$ acting on a bosonic system with a number N of identical particles satisfy the following operator

*These authors contributed equally to this work.

†xint@sustech.edu.cn

‡gllong@tsinghua.edu.cn

relationship [10]:

$$\hat{a}^{\dagger}|N\rangle = \sqrt{N+1}|N+1\rangle,$$
$$\hat{a}|N\rangle = \sqrt{N}|N-1\rangle. \quad (1)$$

Given the importance of the creation and annihilation operators, efficiently performing them in a quantum process is critical. However, implementing such bosonic operations is challenging. Because these operators are nonunitary and inherently probabilistic, they cannot be realized during the Hamiltonian evolution of a physical system without enlarging the Hilbert space.

Ignoring the modification of the probability amplitude of state, the conventional addition and subtraction of a particle can be expressed as

$$\hat{K}^{\dagger}|N\rangle = |N+1\rangle,$$
$$\hat{K}|N\rangle = |N-1\rangle, \quad (2)$$

which can be called addition and subtraction operations.

We consider addition and subtraction operators with identical particle numbers N. Our method can realize the addition operator $\hat{K}^{\dagger}$ and subtraction operator $\hat{K}$ in one quantum circuit.

In our method, the identical particle number N is mapped to a corresponding $|N\rangle$ state. For convenience, we adopt a truncated form of the creation operation $\hat{K}^{\dagger}$ by defining it as an $(N+1)\times(N+1)$ matrix,

$$\hat{K}^{\dagger} = \sum_{i=0}^{N-1} |i+1\rangle\langle i|, \quad \hat{K} = \sum_{i=1}^{N} |i-1\rangle\langle i|. \quad (3)$$

Every operation above can be decomposed into a sum form of two unitary operations:

$$\hat{K}^{\dagger} = \frac{U_0 + U_1}{2}, \quad \hat{K} = \frac{U_2 + U_3}{2}, \quad (4)$$

where

$$U_0 = \sum_{i=0}^{N-1} |i+1\rangle\langle i| + |0\rangle\langle N|,$$
$$U_1 = \sum_{i=0}^{N-1} |i+1\rangle\langle i| - |0\rangle\langle N|,$$
$$U_2 = \sum_{i=1}^{N} |i-1\rangle\langle i| + |N\rangle\langle 0|,$$
$$U_3 = \sum_{i=1}^{N} |i-1\rangle\langle i| - |N\rangle\langle 0|.$$

Considering the fact that the operators $\hat{K}^{\dagger}$ and $\hat{K}$ can be expressed as a linear combination of unitary operators, we can perform the addition and subtraction operators via duality quantum computing [11–14]. In duality quantum computing, the work system with initial state $|\Psi\rangle$ and the d-dimensional ancillary system with initial state $|0\rangle$ are coupled together. The corresponding digital simulation quantum circuit of the addition and subtraction operators from the algorithm is further shown in Fig. 1.

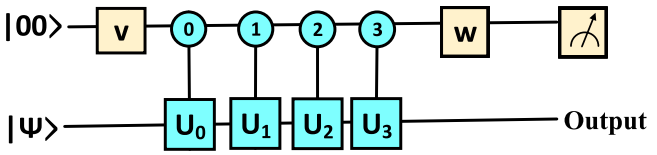

FIG. 1. Quantum circuit of realizing addition and subtraction operators. $|\Psi\rangle$ denotes the initial state of the work system, and $|00\rangle$ is the initial state of the auxiliary system. The squares represent unitary operations, and the circles represent the state of the controlling qubit. Unitary operations U_0, U_1, U_2, and U_3 are activated only when the auxiliary qubit is $|00\rangle$, $|01\rangle$, $|10\rangle$, and $|11\rangle$, respectively. We "read out" the output of the auxiliary system and construct the quantum density matrix of the work system. We can realize the addition operator for the auxiliary system in states $|00\rangle$ and $|01\rangle$ and subtraction operator for the auxiliary system in states $|10\rangle$ and $|11\rangle$.

As shown in Fig. 1, the unitary operators V and W performed on the two-qubit ancillary system are

$$V = H \otimes H, \quad (5)$$

$$W = I \otimes H. \quad (6)$$

The circuit realizes the process

$$|0\rangle_2|\Psi\rangle \rightarrow \sqrt{\frac{1}{2}}\hat{K}^{\dagger}|00\rangle_2|\Psi\rangle + \sqrt{\frac{1}{2}}\hat{K}|10\rangle_2|\Psi\rangle + \sqrt{\frac{1}{2}}\hat{J}^{\dagger}|01\rangle_2|\Psi\rangle + \sqrt{\frac{1}{2}}\hat{J}|11\rangle_2|\Psi\rangle, \quad (7)$$

where the operators $\hat{K}^{\dagger}$, $\hat{K}$, $\hat{J}^{\dagger}$, and $\hat{J}$ act on the work system $|\Psi\rangle$. To be the same as $\hat{K}^{\dagger}$ and $\hat{K}$ in Eq. (7), the operators $\hat{J}^{\dagger}$ and $\hat{J}$ can be calculated by

$$\hat{J}^{\dagger} = \frac{U_0 - U_1}{2} = |0\rangle\langle N|, \quad \hat{J} = \frac{U_2 - U_3}{2} = |N\rangle\langle 0|. \quad (8)$$

The $\hat{J}^{\dagger}$ operation transforms the $|N\rangle$ state into the $|0\rangle$ state, and $\hat{J}$ transforms the $|0\rangle$ state into the $|N\rangle$ state. So it is clear that the operator $\hat{J}^{\dagger}$ is a special addition operator dealing with the maximum state, and the operator $\hat{J}$ is the special subtraction operator dealing with the minimum state. The probabilities of the realization of the addition operator and the subtraction operator are both 50%.

Then we will consider addition and subtraction operations in the case where the identical particle number $N = 3$ in Eq. (4).

III. EXPERIMENT AND RESULT

We experimentally inspect our algorithm using a four-qubit nuclear magnetic resonance (NMR) system. As introduced before, the ancillary system is two qubits, and we also choose a two-qubit work system $|00\rangle$, $|01\rangle$, $|10\rangle$, $|11\rangle$ to represent 0, 1, 2, 3. The four-qubit sample is ^{13}C-labeled *trans*-crotonic acid dissolved in acetone-$d6$. The structure of the molecule is shown in Fig. 2, where C_1 to C_4 denote the four qubits; the first two qubits are the auxiliary system, and the last two qubits are the work system. The methyl group M, H_1, and H_2 were decoupled throughout all experiments. For molecules

	C1	C2	C3	C4
C1	1705.5			
C2	41.64	14558.0	Crotonic Acid	
C3	1.46	69.72	12330.5	
C4	7.04	1.18	72.36	16764.0
T2	0.84	0.92	0.66	0.79

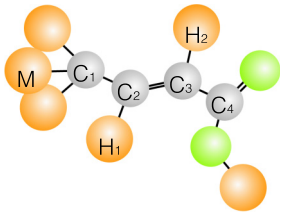

FIG. 2. Molecular structure and Hamiltonian parameters of ^{13}C-labeled *trans*-crotonic acid. C_1, C_2, C_3, and C_4 are used as four qubits. The chemical shifts and J couplings (in Hz) are listed by the diagonal and off-diagonal elements, respectively. T_2 (in seconds) are also shown at the bottom.

in liquid solution, both intramolecular dipolar couplings (between spins in the same molecule) and intermolecular dipolar couplings (between spins in different molecules) are averaged away by the rapid tumbling [15]. The internal Hamiltonian under the weak-coupling approximation is

$$\mathcal{H} = -\sum_{j=1}^{4} \pi \nu_j \sigma_z^j + \sum_{j<k}^{4} \frac{\pi}{2} J_{jk} \sigma_z^j \sigma_z^k, \tag{9}$$

where ν_j is the chemical shift and J_{jk} is the J-coupling strength. All experiments were carried out on a Bruker DRX 400-MHz spectrometer at room temperature (296.5 K).

The entire experiment can be divided into three parts, and the experimental circuits are shown in Fig. 3.

Step 1. Initialization. Starting from the thermal equilibrium state, we drive the system to the pseudopure state (PPS) with the method of the spatial averaging technique [16–21]. Step 1 in Fig. 3 is the experimental circuit realizing the PPS where all local operations are optimized using gradient ascent pulse engineering (GRAPE) with a fidelity greater than 99.5% [22,23]. The final form of the four-qubit PPS is $\rho_{0000} = (1-\epsilon)\mathbb{I}/16 + \epsilon|0000\rangle\langle 0000|$, where $\mathbb{I}$ is the identity matrix and $\epsilon \approx 10^{-5}$ is the polarization. Since only the deviated part $|0000\rangle$ contributes to the NMR signals, the density matrix used in NMR is a deviated matrix, and the PPS is able to serve as an initial state. The experimental results are represented as the density matrices obtained with the state tomography technique [24–26] shown in Fig. 4. The fidelity between the experimental results and $|0000\rangle$ is over 99.02%.

Step 2. Operator. As we introduced in Sec. II, we perform the addition and subtraction operators $\hat{K}^\dagger$ and $\hat{K}$ using duality quantum computing. In this case, C1 and C2 represent the ancillary system with initial state $|0\rangle$, and C3 and C4 represent the work system as shown in Fig. 3. The unitary operators V and W performed on the C1 and C2 system can be realized as shown in step 2 in Fig. 3. Moreover, the four control-U operators can be realized by using the GRAPE technology with a fidelity greater than 99.5%.

Step 3. Measurement. The measurement circuit is also listed in Fig. 3 in step 3. From Eq. (7), we know that the operator applied in the work system depends on the measurement of the ancillary system. So we have to measure the ancillary

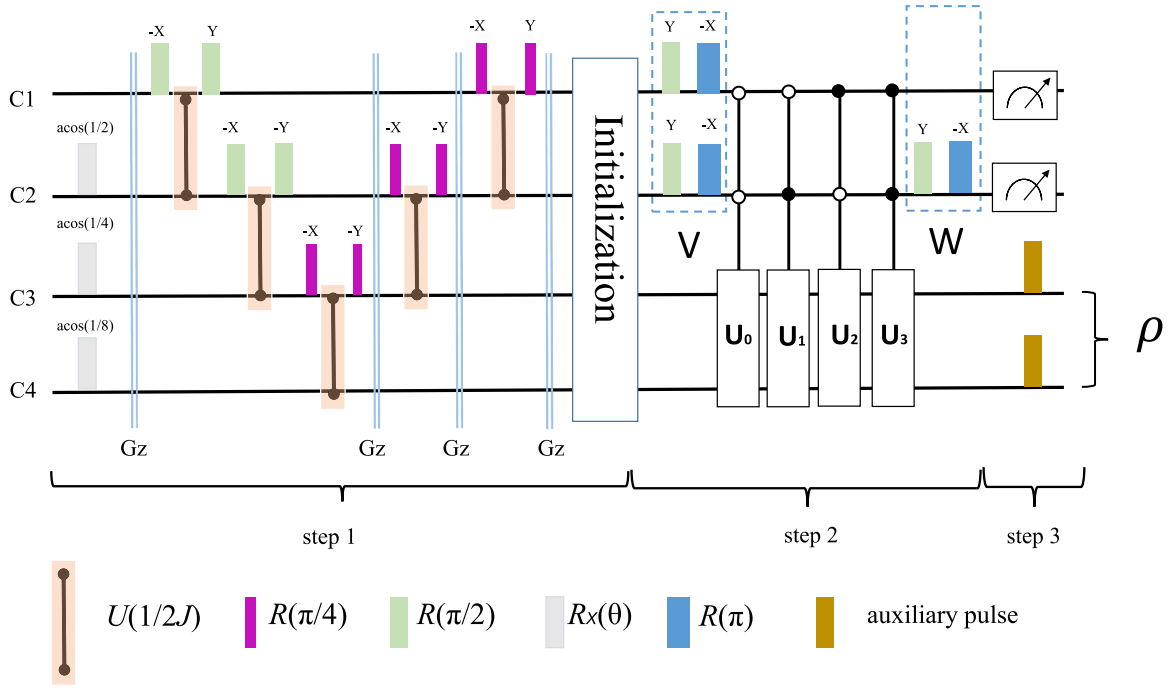

FIG. 3. NMR sequence to realize the addition and subtraction operators. In the first step, we use a spatial averaging method to prepare the pseudopure state. In this part, the purple rectangles stand for the unitary operations which rotate 45° with a coordinate axis. Similarly, the green rectangles rotate 90°. The white rectangles stand for the unitary operations which rotate with the special angle with the X axis. The blue rectangles stand for the unitary operations which rotate 180° with the Y axis. The double straight lines stand for the gradient field in the z direction. In the second step, the radio-frequency pulses during this procedure are optimized using the GRAPE technology to realize the controlled operator. In the third step, we measure the first two qubits and use the quantum tomography technology to obtain the final density matrix. The brown squares are the auxiliary pulse which can be used for quantum tomography.

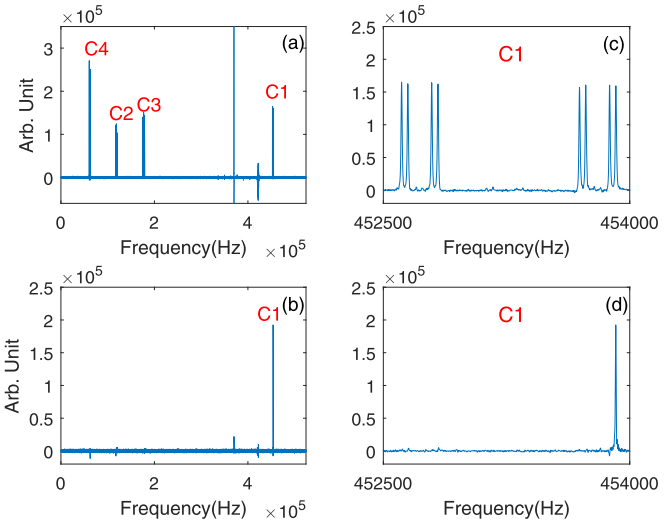

FIG. 4. The spectrum of the thermal equilibrium state and PPS. (a) The spectrum of the thermal equilibrium state. The x axis is the relative frequency, and the y axis is the amplitude in arbitrary units. Since the qubits are all carbon atoms, all signals of these four qubits can be detected through the carbon channel in NMR experiments. (b) The spectrum of spin C1 in the thermal equilibrium state. This is an expanded view of spin C1 in (a). From plot, we can observe more information in detail. The quantum state of the remaining spins (C2, C3 and C4) is as indicated based on J12, J13, and J14 shown in Fig. 2. (c) The spectrum of the PPS. As we know, the ground state $|0000\rangle$ cannot be detected directly in NMR, and we can apply $R_y^i(\pi/2)$ to it to obtain a single peak of the ith spin. In our case, only the peak in the spectrum of C1 can be detected by applying the $R_y^1(\pi/2)$ pulse. (d) The spectrum of spin C1 in the PPS. This is also an expanded view of spin C1 in (c). It is clear that the peaks standing for the quantum state except $|0\rangle$ are close to zero.

qubits and use quantum tomography technology to get the density matrix by applying auxiliary pulses on C3 and C4.

IV. RESULT

Here we introduce two examples in detail with two different initial quantum states to show our algorithm. One is a general quantum state such as $|\phi\rangle = |01\rangle$; the other is a superposition state such as $|\phi\rangle = \frac{|01\rangle+|10\rangle}{2}$. These initial states can be obtained by single-qubit gates and the controlled-NOT (CNOT) gate from the ground state $|00\rangle$. Then we can get the experimental results shown below by following the steps introduced above.

A. General state

The experimental results of the first example are shown in Fig. 5. We find that the addition operation can be realized when the auxiliary qubits are $|00\rangle$. Then we calculate the fidelity, defined as [27]

$$F(\rho,\sigma) = |\mathrm{Tr}(\rho\sigma)|/\sqrt{\mathrm{Tr}(\rho^2)\mathrm{Tr}(\sigma^2)}, \tag{10}$$

where ρ and σ represent the density matrices from the experiments and theories, respectively. So comparing the experiments shown in Fig. 5(b) with the quantum state $|10\rangle$, the fidelity between them is over 98.8%. Thus, we probabilistically

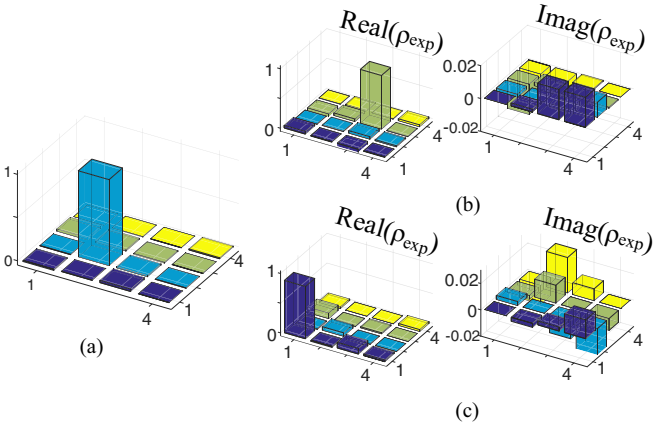

FIG. 5. The density matrix of the initial quantum state and final state (in the normalized units). (a) The initial quantum state $|01\rangle$. (b) The final state when the measurement of ancillary qubits is $|00\rangle$. (c) The final state when the measurement of ancillary qubits is $|10\rangle$. The left part is the real part of the density matrix, and the right part is the imaginary part in (b) and (c).

realize the quantum process

$$\hat{K}^{\dagger}|01\rangle = |10\rangle. \tag{11}$$

Similarly, the subtraction operator can be performed when the auxiliary qubit is $|10\rangle$, as shown in Eq. (8). Comparing the results shown in Fig. 5(c) with theoretical state $|00\rangle$, the fidelity between them is approximately equal to 98.3%. Thus, we also probabilistically realize the quantum process

$$\hat{K}|01\rangle = |00\rangle. \tag{12}$$

We introduce the idea that the addition and subtraction operators can be performed probabilistically. From Eq. (8), the probabilities depend on the experimental results of the auxiliary qubit shown in Table I. The measurement of $|11\rangle$ should be an experimental error. From the results we find that we can perform the addition and subtraction operators for the same probability of 50%.

B. Superposition state

The experimental results for the second example are shown in Fig. 6. Similarly, we find that the addition operation can be realized when the auxiliary qubit is $|00\rangle$. Then we calculate the fidelity using the definition (13).

Comparing the experiments shown in Fig. 6(b) with the quantum state $\frac{|01\rangle+|10\rangle}{2}$, the fidelity between them is over 96.3%. Thus, we realize the quantum process probabilistically:

$$K^{+}\frac{|01\rangle+|10\rangle}{2} = \frac{|10\rangle+|11\rangle}{2}. \tag{13}$$

TABLE I. The measurement of the auxiliary qubit with the general state.

	$\|00\rangle$	$\|10\rangle$	$\|01\rangle$ and $\|11\rangle$
Probability	49.56	49.51%	0.93%

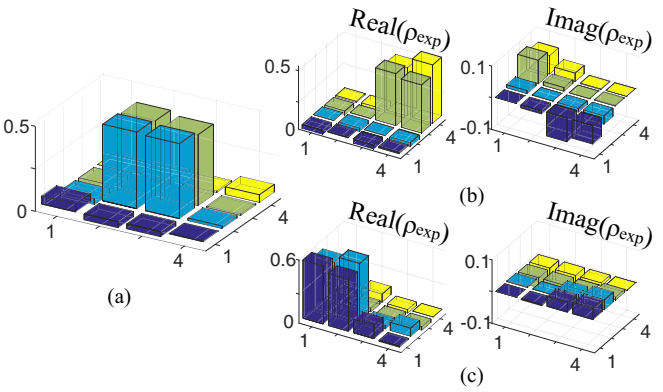

FIG. 6. The density matrix of the initial quantum state and final state (in the normalized units). (a) The initial quantum state $\frac{|01\rangle+|10\rangle}{2}$. (b) The final state when the measurement of ancillary qubits is $|00\rangle$. (c) The final state when the measurement of ancillary qubits is $|10\rangle$. The left part is the real part of the density matrix, and the right part is the imaginary part in (b) and (c).

Similarly, the subtraction operator can be performed when the auxiliary qubit is $|10\rangle$, as shown in Eq. (8). Comparing the results shown in Fig. 6(c) with theoretical state $\frac{|01\rangle+|10\rangle}{2}$, the fidelity between them is approximately equal to 97.0%. Thus, we also realize the quantum process probabilistically:

$$K^{-}\frac{|01\rangle+|10\rangle}{2}=\frac{|00\rangle+|10\rangle}{2}. \tag{14}$$

We introduce the idea that the addition and subtraction operators can be performed probabilistically. From Eq. (8), the probabilities depend on the experimental results of the auxiliary qubit shown in Table II. The measurement of $|11\rangle$ should be an experimental error. From the results we find that we can perform the addition and subtraction operators for the same probability of 50%.

C. Further experiment

show the unique feature of our algorithm, we present the further experiment results of applying addition, subtraction, and U_0 operators on the initial state $(|00\rangle+|01\rangle+|10\rangle+|11\rangle)/2$, in which the quantum state should evolve to different quantum states separately. When we apply the U_0 operator on the initial state, the fidelity between the final state as shown in Fig. 7(b) and the initial state is over 99%. This result also satisfies the theory we introduced before. It is worth emphasizing that the subspace of ancillary qubits will influence the target quantum states according to Eq. (7), and it is the evolution of the quantum state under the four operators in fact. We show the experimental results in Fig. 7 when applying the addition and subtraction operators to the initial state. It is clear that the addition and subtraction

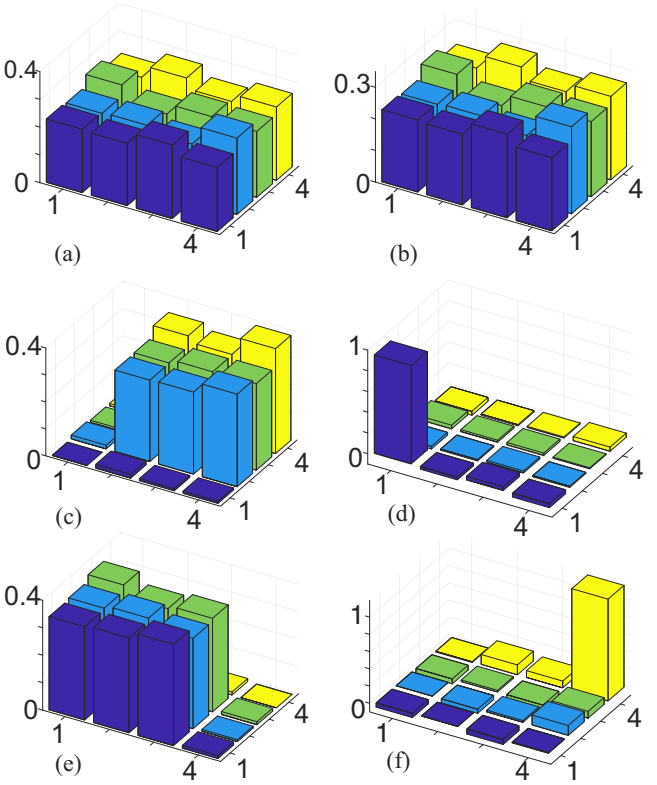

FIG. 7. The real part of the density matrix of the initial quantum state and final state (in the normalized units). (a) The initial quantum state is $(|00\rangle+|01\rangle+|10\rangle+|11\rangle)/2$. We apply the U_0 operator on the initial state; the final state is shown in (b). The results of the work system are shown in (c) when the ancillary qubit subspace is $|00\rangle$. Following the same setups as in the statement above, we realize subtraction operator on the initial state, as shown in (e) when the ancillary qubit subspace is $|10\rangle$. Similarly, we can perform $\hat{J}^{\dagger}$ with the ancillary qubit $|01\rangle$, as shown in (d), and $\hat{J}$ with the ancillary qubit $|11\rangle$, as shown in (f).

operators we realized are nonunitary operators. Thus, we realize the quantum process $\hat{K}^{\dagger}$ as shown in Fig. 7(c), $\hat{K}$ as shown in Fig. 7(e), $\hat{J}^{\dagger}$ as shown in Fig. 7(d), and $\hat{J}$ as shown in Fig. 7(f). The probabilities of measuring the auxiliary system are shown in Table III.

V. APPLICATION

We have presented a universal algorithm to perform addition and subtraction operations using a two-qubit auxiliary system. Our algorithm has many applications, and one of them is quantum random walks [28]. Quantum random walks (QRWs) are extensions of the classical counterparts and have wide applications in quantum algorithms [29], quantum simulation [30], quantum computation [31], and so on [32].

TABLE II. The measurement of the auxiliary qubit with the superposition state.

	$\|00\rangle$	$\|10\rangle$	$\|01\rangle$ and $\|11\rangle$
Probability	48.84%	49.79%	1.38%

TABLE III. The measurement of the auxiliary qubit in the further experiment.

	$\|00\rangle$	$\|10\rangle$	$\|01\rangle$	$\|11\rangle$
Probability	38.72%	13.96%	36.78%	10.54%

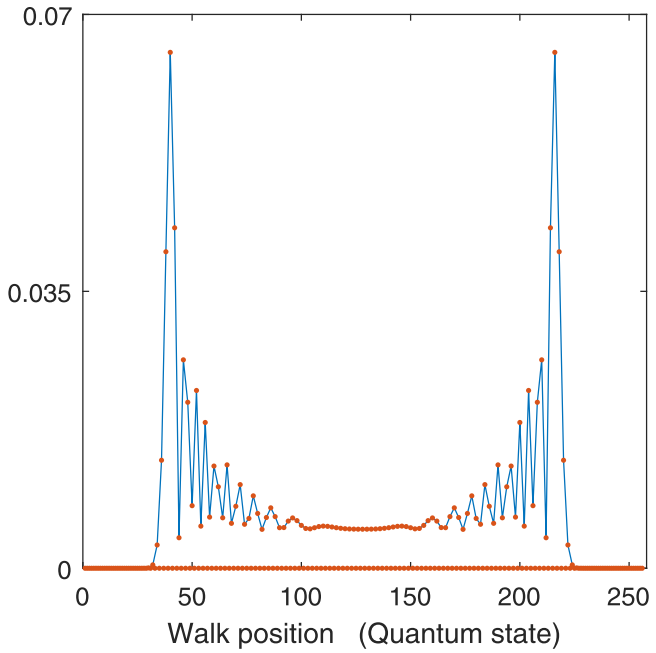

FIG. 8. The simulation of a quantum random walk when the initial state is $|01000000\rangle$ (128). The x axis represents the quantum state, from $|00000000\rangle$ (0) to $|11111111\rangle$ (255). The y axis represents the measurement probabilities (in the normalized units). The solid circles are the probabilities of each state. The statistical distribution can be observed by the line linked by the nonzero circles.

In standard one-dimensional discrete-time quantum walks (DTQWs), the walker's position can be denoted as $|x\rangle$ (x is an integer), and the coin can be described with the basis states $|0\rangle$ and $|1\rangle$ [33,34]. The evolutions of the walker and the coin are usually characterized by a time-independent unitary operator $U = TS_c|\phi\rangle$. In each step, the coin is tossed by

$$S_c(\phi) = \begin{pmatrix} \cos(\phi) & -\sin(\phi) \\ \sin(\phi) & \cos(\phi) \end{pmatrix}, \tag{15}$$

where ϕ is the rotation angle and equal to 45° in this work. The walker is shifted by $T = \Sigma|x+1\rangle\langle x| \otimes |1\rangle\langle 1| + \Sigma|x-1\rangle\langle x| \otimes |0\rangle\langle 0|$. In general, the result of the DTQWs with a finite number of steps is determined by the initial states of the coin and the walker as well as the operator U. Obviously, the operator U can be realized by the algorithm we introduced above. The operator $|x+1\rangle\langle x| \otimes |1\rangle\langle 1|$ is the addition operator when the measurement of the first auxiliary qubit is $|1\rangle$. Similarly, the operator $|x-1\rangle\langle x| \otimes |0\rangle\langle 0|$ is the addition operator when the measurement of the first auxiliary qubit is $|0\rangle$. So the first auxiliary qubit of our algorithm can be considered the coin qubit of QRWs. Then we present two kinds of simulations with different initial states to demonstrate the QRWs with our algorithm. The size of the work system we choose is eight-qubit system, and the auxiliary system is still a two-qubit system. The random-walk step is 128, and that means we repeat the circuit in Fig. 1 a total of 128 times. The demonstration results with initial state $|01000000\rangle$ are shown in Fig. 8. We find that the probabilities of the odd state are all zero, and only the even state has the probability to find the particle. Moreover,

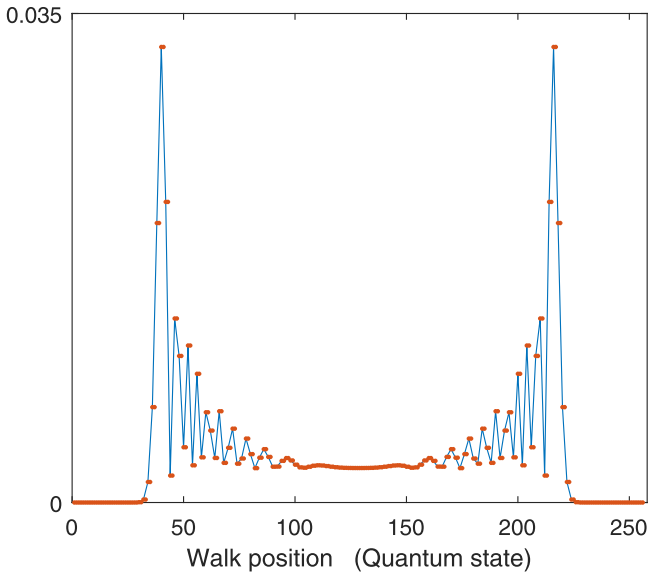

FIG. 9. The simulation of a quantum random walk when the initial state is $\frac{|01000000\rangle+|01000001\rangle}{2}$ (128, 129). The x axis represents the quantum state, from $|00000000\rangle$ (0) to $|11111111\rangle$ (255). The y axis represents the measurement probabilities (in the normalized units). The solid circles are the probabilities of each state. The statistical distribution can be observed by the line linked by all the circles.

the statistical distribution has good agreement with theory [34]. As we introduced before, our algorithm can be applied to the supposition state, so we choose another initial state, $\frac{|01000000\rangle+|01000001\rangle}{2}$; the simulation result is shown in Fig. 9. Obviously, now the odd state and even state have the same probability, and the statistical distribution stays constant.

VI. CONCLUSION

In summary, we proposed a universal algorithm to realize addition and subtraction operators. In this algorithm addition and subtraction operations can be performed by the linear combination of unitary operations with a two-qubit ancillary system. Moreover, the number of ancillary qubits is independent of the size of the work system. We implemented this algorithm in a four-qubit NMR quantum processor. Since two qubits are the ancillary system, the work system was evaluated in a four-dimensional Hilbert space. Without loss of generality, we chose two different initial quantum states to prove our algorithm. Our experimental results have shown good agreement with the theoretical predictions. Moreover, the method which realizes addition and subtraction operators can be employed to perform a quantum random walk in an arbitrary initial state. Our algorithm can provide universal quantum control technology which can also be utilized in other quantum physical systems such as a nitrogen-vacancy center, a superconducting, trapped ion, etc.

ACKNOWLEDGMENTS

This work was supported by the National Basic Research Program of China (Grant No. 2015CB921002), the

National Natural Science Foundation of China (Grants No. 11175094 and No. 91221205), the National key Research and Development Program of China (Grants No. 2017YFA0303700); Beijing Advanced Innovation Center for future Chip (ICFC). T.X. is supported by the Science, Technology and Innovation Commission of Shenzhen Municipality (Grants No. ZDSYS20170303165926217 and No. JCYJ20170412152620376) and the Guangdong Innovative and Entrepreneurial Research Team Program (Grant No. 2016ZT06D348).

[1] J. J. Sakurai, S. F. Tuan, and E. D. Commins, Modern quantum mechanics, revised edition, Am. J. Phys. **63**, 93 (1995).

[2] V. V. Borzov and E. V. Damaskinsky, Realization of the annihilation operator for an oscillator-like system by a differential operator and Hermite-Chihara polynomials, Integral Transform. Spec. Funct. **13**, 547 (2002).

[3] A. I. Maalouf and I. R. Petersen, Coherent control for a class of annihilation operator linear quantum systems, IEEE Trans. Autom. Control **56**, 309 (2011).

[4] V. Parigi, A. Zavatta, M. Kim, and M. Bellini, Probing quantum commutation rules by addition and subtraction of single photons to/from a light field, Science **317**, 1890 (2007).

[5] I. Urizar-Lanz and G. Tóth, Number-operator–annihilation-operator uncertainty as an alternative for the number-phase uncertainty relation, Phys. Rev. A **81**, 052108 (2010).

[6] J. S. Lundeen and K. J. Resch, Practical measurement of joint weak values and their connection to the annihilation operator, Phys. Lett. A **334**, 337 (2005).

[7] C. Hempel, C. Maier, J. Romero, J. McClean, T. Monz, H. Shen, P. Jurcevic, B. P. Lanyon, P. Love, R. Babbush *et al.*, Quantum Chemistry Calculations on a Trapped-Ion Quantum Simulator, Phys. Rev. X **8**, 031022 (2018).

[8] S. S. Mizrahi and V. V. Dodonov, Creating quanta with "annihilation" operator, J. Phys. A **35**, 8847 (2012).

[9] M. Um, J. Zhang, D. Lv, Y. Lu, S. An, J. N. Zhang, H. Nha, M. S. Kim, and K. Kim, Phonon arithmetic in a trapped ion system, Nat. Commun. **7**, 11410 (2016).

[10] S. N. Bose, Plancks gesetz und lichtquantenhypothese, Z. Phys. **26**, 178 (1924).

[11] G. L. Long, General quantum interference principle and duality computer, Commun. Theor. Phys. **45**, 825 (2006).

[12] S. Gudder, Mathematical theory of duality quantum computers, Quant. Inf. Process. **6**, 37 (2007).

[13] S. J. Wei, D. Ruan, and G. L. Long, Duality quantum algorithm efficiently simulates open quantum systems, Sci. Rep. **6**, 30727 (2016).

[14] S. J. Wei and G. L. Long, Duality quantum computer and the efficient quantum simulations, Quant. Inf. Process. **15**, 1189 (2016).

[15] L. M. K. Vandersypen and I. L. Chuang, NMR techniques for quantum control and computation, Rev. Mod. Phys. **76**, 1037 (2005).

[16] D. G. Cory, A. F. Fahmy, and T. F. Havel, Ensemble quantum computing by NMR spectroscopy, Proc. Natl. Acad. Sci. U.S.A. **94**, 1634 (1997).

[17] D. Lu, N. Xu, R. Xu, H. Chen, J. Gong, X. Peng, and J. Du, Simulation of Chemical Isomerization Reaction Dynamics on a NMR Quantum Simulator, Phys. Rev. Lett. **107**, 020501 (2011).

[18] Y. Lu, G. R. Feng, Y. S. Li, and G. L. Long, Experimental digital quantum simulation of temporal–spatial dynamics of interacting fermion system, Sci. Bull. **60**, 241 (2015).

[19] T. Xin, H. Li, B. X. Wang, and G. L. Long, Realization of an entanglement-assisted quantum delayed-choice experiment, Phys. Rev. A **92**, 022126 (2015).

[20] J. Pearson, G. R. Feng, C. Zheng, and G. L. Long, Experimental quantum simulation of Avian Compass in a nuclear magnetic resonance system, Sci. China Phys. **59**, 120312 (2016).

[21] K. Li, G. Long, H. Katiyar, T. Xin, G. Feng, D. Lu, and R. Laflamme, Experimentally superposing two pure states with partial prior knowledge, Phys. Rev. A **95**, 022334 (2017).

[22] N. Khaneja, T. Reiss, C. Kehlet, T. Schulte-Herbrüggen, and S. J. Glaser, Optimal control of coupled spin dynamics: design of NMR pulse sequences by gradient ascent algorithms, J. Magn. Reson. **172**, 296 (2005).

[23] C. A. Ryan, C. Negrevergne, M. Laforest, E. Knill, and R. Laflamme, Liquid-state nuclear magnetic resonance as a testbed for developing quantum control methods, Phys. Rev. A **78**, 012328 (2008).

[24] I. L. Chuang, L. M. K. Vandersypen, X. Zhou, D. W. Leung, and S. Lloyd, Experimental realization of a quantum algorithm, Nature (London) **393**, 143 (1998).

[25] I. L. Chuang, N. Gershenfeld, and M. Kubinec, Experimental Implementation of Fast Quantum Searching, Phys. Rev. Lett. **80**, 3408 (1998).

[26] I. L. Chuang, N. Gershenfeld, M. G. Kubinec, and D. W. Leung, Bulk quantum computation with nuclear magnetic resonance: theory and experiment, Phys. Eng. Sci. **454**, 447 (1998).

[27] Y. S. Weinstein, M. A. Pravia, E. M. Fortunato, S. Lloyd, and D. G. Cory, Implementation of the Quantum Fourier Transform, Phys. Rev. Lett. **86**, 1889 (2001).

[28] Y. Aharonov, L. Davidovich, and N. Zagury, Quantum random walks, Phys. Rev. A **48**, 1687 (1993).

[29] N. Shenvi, J. Kempe, and K. B. Whaley, Quantum random-walk search algorithm, Phys. Rev. A **67**, 052307 (2003).

[30] A. Peruzzo, M. Lobino, J. C. F. Matthews, N. Matsuda, A. Politi, K. Poulios, X. Zhou, Y. Lahini, N. Ismail, K. Wörhoff *et al.*, Quantum walks of correlated photons, Science **329**, 1500 (2010).

[31] A. M. Childs, Universal Computation by Quantum Walk, Phys. Rev. Lett. **102**, 180501 (2009).

[32] P. Kurzynski and A. Wojcik, Quantum Walk as a Generalized Measuring Device, Phys. Rev. Lett. **110**, 200404 (2013).

[33] J. Kempe, Quantum random walks: An introductory overview, Contemp. Phys. **44**, 307 (2003).

[34] S. E. Venegas-Andraca, Quantum walks: a comprehensive review, Quantum Inf. Process. **11**, 1015 (2012).